INTERNATIONAL JOURNAL FOR NUMERICAL METHODS IN ENGINEERING
Int. J. Numer. Meth. Engng. **46**, 409–431 (1999)

AN ENHANCED PIPE ELBOW ELEMENT—APPLICATION IN PLASTIC LIMIT ANALYSIS OF PIPE STRUCTURES

A. M. YAN[1,*], R. J. JOSPIN[2] AND D. H. NGUYEN[1]

[1] *LTAS-University of Liege, Rue Ernest Solvay 21, 4000-Liege, Belgium*
[2] *CNEN-Instituto de Engenharia Nuclear, P.O. Box 68550, 21945-970 Rio de Janeiro, Brazil*

SUMMARY

In this paper, we present a new pipe elbow element based on a previous simplified model proposed by Bathe and Almeida [1, 2] and modified by Militello and Huespe [3]. It is really a beam-type element but it describes the ovalization, warping, radial expansion and non-symmetric deformation of cross-section of curved pipe with Fourier series. Therefore, it could model precisely enough a real pipe elbow structure but remains simple. The extensive loading cases are effectively implemented by the proposed numerical techniques and displacement model. The developed element is used in this paper in plastic limit analysis of pipe elbow structures. This is realized by means of a direct mathematical programming technique. Various elastic and plastic limit state analyses of straight pipes and elbow structures are presented, which illustrates the efficiency of the element and the numerical method. Copyright © 1999 John Wiley & Sons, Ltd.

KEY WORDS: pipe elbow finite element; pipe structure analysis; limit analysis; mathematical programming technique

1. INTRODUCTION

The structural integrity of pipelines is of major concern in the nuclear, oil and other industries. Due to the complexity of geometry and loading of pipe elbow, even a usual linear analysis with tri-dimensional or general shell elements is expensive. The data preparation is usually time-consuming. The non-linear plastic analysis is certainly more difficult. Hence, some simplified finite elements were proposed, among which the elbow element proposed by Bathe and Almeida [1, 2] was most interesting due to its simplicity and effectiveness. It is a beam model and the ovalization of curved pipe is described by finite Fourier series following von Karman's pioneering work. This element was modified later by Militello and Huespe [3] in order to include the warping deformation and to improve the inter-element continuity. However, it has been noticed that some important drawbacks and limitations remain with this element. In some situations, it leads to important deviations in computation from real behaviour of pipe structure. Furthermore some loading cases could not be correctly dealt with.

In this paper, we try to improve and develop this pipe elbow element in order to make it useful in all possible loading cases and to ensure a satisfactory precision for elastic analysis and also for non-linear plastic limit analysis via a mathematical programming technique. The plastic limit

* Correspondence to: A. M. Yan, LTAS-Fracture Mechanics, University of Liege, Rue Ernest Solvay 21, B-4000 Liege, Belgium. E-mail: an-yan@ulg.ac.be

CCC 0029-5981/99/270409–23$17.50

Received 25 August 1998
Revised 20 January 1999

load of structures is found by a minimization procedure when the structure is discretized by finite elements. This is a direct method based on Markov's variational principle; cf. [4]. The numerical results show that this enhanced pipe elbow element provides an effective tool to carry out accurately elastic and plastic limit analysis of pipe structures under complex loading at low computing costs.

2. IMPROVEMENT OF DISPLACEMENT MODEL OF ELBOW ELEMENT

2.1. *Representation of elbow geometry* [1]

The element geometry is described through an interpolation of node co-ordinate $\mathbf{X}^k = (X, Y, Z)$ along the pipe axis and a unit direction vector $({}^0\mathbf{V}_r^k, {}^0\mathbf{V}_s^k, {}^0\mathbf{V}_t^k)$ which defines the pipe axis $X^0 = (r, s, t)$ at node k $(k = 1, 4)$. It obeys the following relation:

$$\mathbf{X}(r, s, t) = \sum_{k=1}^{4} L_k(r)\mathbf{X}^k + t\sum_{k=1}^{4} a_k L_k(r)\ {}^0\mathbf{V}_t^k + s\sum_{k=1}^{4} a_k L_k(r)\ {}^0\mathbf{V}_s^k \tag{1}$$

where r, s, t are the isoparametric co-ordinates, L_k the Lagrange's interpolation functions [1] and a_k the radius of the pipe section at node k (see Figure 1).

2.2. *Approximation of the displacement field*

The displacement field $\mathbf{u}$ of the elbow surface is composed of two displacement fields:

$$\mathbf{u} = \mathbf{u}^{\mathrm{b}} + \mathbf{u}^{\mathrm{c}} \tag{2}$$

The beam displacement field $\mathbf{u}^{\mathrm{b}} = (u_x, u_y, u_z)$ verifies Bernoulli's hypothesis by using the relation

$$\mathbf{u}^{\mathrm{b}} = \sum_{k=1}^{4} L_k(r)\mathbf{U}^k + t\sum_{k=1}^{4} a_k L_k(r)\mathbf{V}_t^k + s\sum_{k=1}^{4} a_k L_k(r)\mathbf{V}_s^k \tag{3a}$$

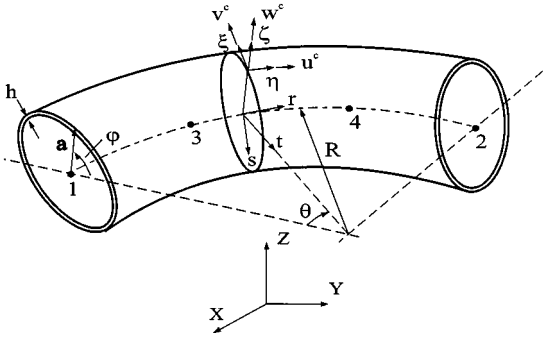

Figure 1. Elbow geometry and axis systems (1 element with 4 nodes)

where $\mathbf{U}^k = (U_X, U_Y, U_Z)$ is the displacement of the pipe axis at node k;

$$\mathbf{V}_s^k = \mathbf{\Phi}^k \times {}^0\mathbf{V}_s^k, \quad \mathbf{V}_t^k = \mathbf{\Phi}^k \times {}^0\mathbf{V}_t^k \tag{3b}$$

with $\mathbf{\Phi}^k = (\Phi_x, \Phi_y, \Phi_z)$, the vector representing the rotation of the cross-section.

The complementary displacement field $\mathbf{u}^c = (u^c, v^c, w^c)$ representing ovalization, distortion (warping) and non-symmetric radial deformation of the cross-section, is developed in hoop direction φ by a Fourier series:

$$u^c = \sum_k^4 \left[\sum_{n=2}^{N_f} (u_n^s)_k L_k(r) \cos n\varphi + \sum_{n=2}^{N_g} (u_n^a)_k L_k(r) \sin n\varphi \right] \tag{4}$$

$$v^c = \sum_{k=1}^{2} \left[\sum_{m=1}^{N_p} [(v_n^s)_k H_k(r) + (v_{n,r}^s)_k h_k(r)] \sin n\varphi + \sum_{m=1}^{N_q} [(v_n^a)_k H_k(r) + (v_{n,r}^a)_k h_k(r)] \cos n\varphi \right] \tag{5}$$

where $n = 2m$ and $v_{,r} = \mathrm{d}v^c/\mathrm{d}r$,

$$w^c = -\frac{\partial v^c}{\partial \varphi} + w_0^s + w_1^s \cos\varphi + w_1^a \sin\varphi \tag{6a}$$

with

$$w_i^j = \sum_{k=1}^{2} [(w_i^j)_k H_k(r) + (w_{i,r}^j)_k h_k(r)], \quad w_{,r} = \frac{\mathrm{d}w^c}{\mathrm{d}r} \tag{6b}$$

$i = 0, 1$ for $j = \mathrm{s}$ (in symmetric case) and $i = 1$ for $j = \mathrm{a}$ (in antisymmetric case). H_k, h_k are the third-order Hermite interpolation functions introduced by Militello and Huespe [3]; u_n^s, v_n^s, w_n^s, u_n^a, v_n^a, w_n^a, are the symmetric (s) and anti-symmetric (a) displacement components corresponding to the harmonic n.

In (4)–(6), the Fourier series for ovalization and warping begins with harmonics $n = 2$ since the terms 0 and 1 have been taken into account by the beam displacements assuming that the cross-section remains plane. In fact, we show in Figure 2 the following.

Warping terms:

$$n = 0, \quad u^c = \sum_{k=1}^{4} L_k(r) u_0^k \quad \text{corresponds to } U_r$$

$$n = 1, \quad u^c = \sum_{k=1}^{4} L_k(r) [(u_1^s)^k \cos\varphi + (u_1^a)^k \sin\varphi] \quad \text{corresponds to } \Phi_s, \Phi_t$$

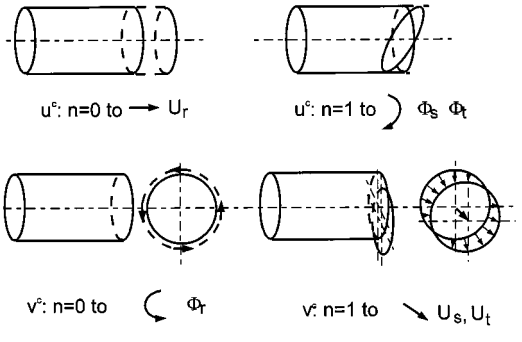

Figure 2. Beam displacement model

Ovalization terms:

$$n = 0, \quad v^{c} = \sum_{k=1}^{2} [v_0 H_k(r) + v_{0,r} h(r)] \quad \text{corresponds to } \Phi_r$$

$$n = 1,\ v^{c} = \sum_{k=1}^{2} \{[(v_1^{s})^k H_k(r) + (v_{1,r}^{s})^k h(r)] \sin\varphi + [(v_1^{a})^k H_k(r) + (v_{1,r}^{a})^k h(r)] \cos\varphi\} \quad \text{corresponds to } U_s,\ U_t$$

The above displacement mode (6) presents an important improvement concerning the radial displacement of pipe in comparison with the work of Bathe and Almeida [1, 2] and Militello and Huespe [3]. Instead of (6), they adopted a hypothesis of inextensibility of the mid-surface of pipe by using following relation

$$w^{c} = -\frac{\partial v^{c}}{\partial \varphi} \tag{7}$$

Consequently, there exist two drawbacks in using their elements:

1. Firstly, they cannot take into account the extension of mid-surface of pipe due to thermal loading, internal pressure. These kinds of loading are frequent in practical engineering. Being inspired by the work of Almeida [5], Jospin [6] proposed a radial expansion term by using harmonic $n = 0$ in (6). The inextensibility condition is excluded. Therefore, the calculation of internal pressure, circular loading and thermal load becomes possible.
2. Secondly, they cannot take into account the non-symmetric deformation of the cross-section of the pipe due to non-axisymmetric loading or due to the geometrical effect of a curved pipe. The geometrical effect of a curved pipe will be illustrated in Section 3.3. The non-axisymmetric loading may be a transverse load or a bending moment. An example is shown in Figure 3 (where the rotation of the section is not represented).

We can illustrate physically that the non-symmetrical deformation of the cross-section is due to Poisson's effect: axial strain ε_η will result in circumferential strain $\varepsilon_\xi = v\varepsilon_\eta$, where v is Poisson's ratio. By consequence, the non-axisymmetric axial strain of bending leads to non-axisymmetric circumferential strain as shown in Figure 3. A numerical example for it will be presented in Section 5.1. Bathe-Almeida's elemental model does not permit this type of deformation. So their displacement model is too rigid and leads to non-negligible numerical error if non-axisymmetric loading exists. It should be pointed out that the non-symmetric *deformation* field in Figure 3 is different from the *displacement* field (U_s, U_t) shown in Figure 2, and it cannot be described by using harmonic term of $n = 1$ for ovalization v. This fact could be seen from the used strain equations (14) and (15). We will show that with the present new displacement model (6), the above two drawbacks of the element are overcome.

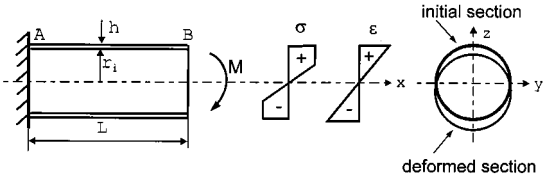

Figure 3. Non-axisymmetric deformation of pipe under bending

2.3. Field of infinitesimal strain

Based on the hypothesis of infinitesimal strain, the strain vector $\boldsymbol{\varepsilon}$ may be considered as the superposition of the strains due to the displacement fields $\mathbf{u}^{\mathrm{b}}$ and $\mathbf{u}^{\mathrm{c}}$. The relation of displacement and strain is presented in the following matrix form:

$$\boldsymbol{\varepsilon} = \begin{bmatrix} \varepsilon_{\eta\eta} \\ \gamma_{\eta\xi} \\ \gamma_{\eta\zeta} \\ \varepsilon_{\xi\xi} \end{bmatrix} = \mathbf{B}\mathbf{q} = [\mathbf{B}^{\mathrm{b}}\mathbf{B}^{\mathrm{c}}] \begin{bmatrix} \mathbf{q}^{\mathrm{b}} \\ \mathbf{q}^{\mathrm{c}} \end{bmatrix} \tag{8}$$

The beam strain matrix $\mathbf{B}^{\mathrm{b}}$ has been given in the work of Bathe and Almeida [1]. The matrix $\mathbf{B}^{\mathrm{c}}$ can be obtained through the infinitesimal strain relation of the Kirchhoff–Love shell. By separating strains into the components of membrane and of flexion according to Novozhilov [7] and Washizu [4], one can deduce the following expressions for a thin-walled pipe elbow ($h/a \ll 1$).

$$\varepsilon_{\eta\eta} = E_{\eta}^{\mathrm{m}} + \zeta E_{\eta}^{\mathrm{f}} \tag{9}$$

$$\varepsilon_{\xi\xi} = E_{\xi}^{\mathrm{m}} + \zeta E_{\xi}^{\mathrm{f}} \tag{10}$$

$$\varepsilon_{\eta\xi} = E_{\eta\xi}^{\mathrm{m}} + \zeta E_{\eta\xi}^{\mathrm{f}} \tag{11}$$

$$E_{\eta}^{\mathrm{m}} = \frac{1}{(R - a\cos\varphi)}\left(\frac{\partial u^{\mathrm{c}}}{\partial\theta} + v^{\mathrm{c}}\sin\varphi - w^{\mathrm{c}}\cos\varphi\right) \tag{12}$$

$$E_{\eta}^{\mathrm{f}} = -\frac{1}{(R - a\cos\varphi)^2}\left(\frac{\partial u^{\mathrm{c}}}{\partial\theta}\cos\varphi + \frac{\partial^2 w^{\mathrm{c}}}{\partial\theta^2}\right) + \frac{\sin\varphi}{(R - a\cos\varphi)a}\left(v^{\mathrm{c}} - \frac{\partial w^{\mathrm{c}}}{\partial\theta}\right) \tag{13}$$

$$E_{\xi}^{\mathrm{m}} = \frac{1}{a}\left(\frac{\partial v^{\mathrm{c}}}{\partial\varphi} + w^{\mathrm{c}}\right) \tag{14}$$

$$E_{\xi}^{\mathrm{f}} = \frac{1}{a^2}\left(\frac{\partial v^{\mathrm{c}}}{\partial\varphi} - \frac{\partial^2 w^{\mathrm{c}}}{\partial\varphi^2}\right) \tag{15}$$

$$E_{\eta\xi}^{\mathrm{m}} = \frac{1}{a}\frac{\partial u^{\mathrm{c}}}{\partial\varphi} + \frac{1}{R - a\cos\varphi}\left(\frac{\partial v^{\mathrm{c}}}{\partial\theta} - u\sin\varphi\right) \tag{16}$$

$$E_{\eta\xi}^{\mathrm{f}} = \frac{1}{(R - a\cos\varphi)^2}\left(u\cos\varphi + \frac{\partial w^{\mathrm{c}}}{\partial\theta}\right) + \frac{1}{(R - a\cos\varphi)a} \times \left(-\frac{\partial u^{\mathrm{c}}}{\partial\theta}\cos\varphi + \frac{\partial v^{\mathrm{c}}}{\partial\theta} - \frac{\partial^2 w^{\mathrm{c}}}{\partial\varphi\partial\theta}\right) \tag{17}$$

By introducing the displacement field defined in (4)–(6) into (9)–(17), we can deduce the components of matrix $\mathbf{B}^{\mathrm{c}}$ corresponding to v^{c}, u^{c} and w^{c}, respectively as (18), the detail of which is presented in [8]:

$$\mathbf{B}_k^{\mathrm{c}} = [\mathbf{B}_v^{\mathrm{s}}\ \mathbf{B}_v^{\mathrm{a}}\ \mathbf{B}_{v,r}^{\mathrm{s}}\ \mathbf{B}_{v,r}^{\mathrm{a}}\ \mathbf{B}_u^{\mathrm{s}}\ \mathbf{B}_u^{\mathrm{a}}\ \mathbf{B}_w^{\mathrm{s}}\ \mathbf{B}_w^{\mathrm{a}}\ \mathbf{B}_{w,r}^{\mathrm{s}}\ \mathbf{B}_{w,r}^{\mathrm{a}}] \tag{18}$$

If we take three terms of Fourier series as examples, equation (18) corresponds to the following generalized shell displacement variables.

(a) if $k = 1, 2$ (end nodes):

$$\mathbf{q}_k^c = [v_2^s v_4^s v_6^s v_2^a v_4^a v_6^a (v,_r)_2^s (v,_r)_4^s (v,_r)_6^s (v,_r)_2^a (v,_r)_4^a (v,_r)_6^a u_2^s u_3^s u_4^s u_2^a u_3^a u_4^a w_0^s w_1^s w_1^a (w,_r)_0^s (w,_r)_1^s (w,_r)_1^a]_k^T \tag{19a}$$

(b) if $k = 3, 4$ (mid-nodes)

$$\mathbf{q}_k^c = [u_2^s \;\; u_3^s \;\; u_4^s \;\; u_2^a u_3^a \;\; u_4^a]_k^T \tag{19b}$$

As we see, there are at least six degrees of freedom (d.o.f) for each node corresponding to the beam model (3), but this number may increase to the maximum of 30 for end nodes (or 12 for mid-nodes) if necessary. Besides, it may be necessary to use also odd terms of harmonic of ovalization for a highly curved elbow. The reasonable selection of d.o.f was discussed in [1, 8].

3. EFFECTS OF INTERNAL PRESSURE ON A CURVED PIPE

In this section we discuss particularly the effect of internal pressure on a curved pipe. It is known that internal pressure will cause radial expansion of pipes and a non-uniform stress distribution in the cross-section due to geometric effects of the elbow. This leads to a reduction of the bearing-load capacity of the elbow. However, the pressure has in the mean time another effect of restitution. Namely, it can increase the stiffness of thin-walled elbow and decrease the ovalization caused by other loads to increase to some extent the bearing-load limit of the elbow. These effects, not yet included in the above element formulation, will be considered in the following development.

3.1. Virtual work principle for a pipe elbow under internal pressure

Consider a curved pipe subjected to external loading ($\mathbf{t}$, $\mathbf{f}$). The virtual work principle represents an equality between the variations of internal virtual strain energy and external virtual work:

$$\int_V \boldsymbol{\sigma}^T \delta\boldsymbol{\varepsilon} \, dV = \int_{\Gamma_t} \mathbf{t}^T \delta\mathbf{u} \, d\Gamma + \int_V \mathbf{f}^T \delta\mathbf{u} \, dV \tag{20}$$

where $\boldsymbol{\sigma}$ and $\boldsymbol{\epsilon}$ are, respectively, the stress and strain tensors, $\mathbf{u}$ is the displacement vector and $\mathbf{t}$, $\mathbf{f}$ are respectively surface and volume loads. By the discretization of structure in finite elements, the virtual elastic strain energy takes the following form:

$$\delta W_{\text{in}} = \delta\mathbf{q}^T \mathbf{K} \mathbf{q} \tag{21}$$

and the external virtual work is

$$\delta W_{\text{ex}} = \delta\mathbf{q}^T \mathbf{g} \tag{22}$$

with

$$\mathbf{K} = \sum_e (\mathbf{L}_e)^T \mathbf{K}_e \mathbf{L}_e, \quad \mathbf{K}_e = \int_{V_e} \mathbf{B}^T \mathbf{D} \mathbf{B} \, dV \tag{23}$$

$$\mathbf{L}_e \mathbf{q} = \mathbf{q}_e \tag{24}$$

where $\mathbf{q}$ and $\mathbf{q}_e$ are respectively the global and elemental displacement vector, $\mathbf{g}$ is the general loading vector, $\mathbf{L}_e$ is the mapping matrix from global to elemental d.o.f., $\mathbf{D}$ is the inverse of the elastic matrix, and $\mathbf{K}$ and $\mathbf{K}_e$ are, respectively, the global and elemental stiffness matrix.

Now let us consider a curved pipe subjected to internal pressure p. Two effects of the pressure will be taken into account: (a) the uniform extension of cross-section represented by radial displacement field in terms of w^0 in (6); and (b) the restitution of the ovalized and distorted cross-section. The first effect contributes to weaken the structure and corresponds to the linear part of the pressure work. On the contrary, the second effect may stiffen the elbow system and corresponds to the non-linear part of the pressure work. We represent the virtual work of the pressure in the following equation:

$$\delta W_{ep} = \int_S p\mathbf{n}^{\mathrm{T}} \delta \mathbf{u}^{\mathrm{c}} \, \mathrm{d}S \tag{25}$$

where one defines S as the deformed elbow surface on which the pressure is applied and $\bar{\mathbf{n}}$ is its normal vector. The product $\bar{\mathbf{n}}\,\mathrm{d}S$ depends on the deformation field of the elbow surface. Considering a transformation from the integration on the deformed configuration S to that on the initial one S_0, we can write (25) in the following form [9]:

$$\delta W_{ep} = \int_{S_0} p\{-E_{31}\delta u - E_{32}\delta v + (1 + E_{11} + E_{22})\delta w\} \, \mathrm{d}S_0 \tag{26}$$

Substituting the components E_{ij} of the deformation tensor defined in [4, 7], we can separate the virtual work of the pressure into two parts:

$$\delta W_{ep} = \delta W_{ep}^{\mathrm{l}} + \delta W_{ep}^{\mathrm{nl}} \tag{27}$$

where $\delta W_{ep}^{\mathrm{l}}$ is the linear part of virtual work of the pressure:

$$\delta W_{ep}^{\mathrm{l}} = \int_{S_0} p\delta w \, \mathrm{d}S_0 \quad \text{or} \quad W_{ep}^{\mathrm{l}} = \int_{S_0} p\delta w \, \mathrm{d}S_0 \tag{28}$$

and $\delta W_{ep}^{\mathrm{nl}}$ is the non-linear part of virtual work of the pressure:

$$\begin{aligned}\delta W_{ep}^{\mathrm{nl}} = \int_{S_0} p\Bigg[&\left(\frac{u}{R_1} - \frac{1}{A_1}\frac{\partial w}{\partial \alpha_1}\right)\delta u + \left(\frac{v}{R_2} - \frac{1}{A_2}\frac{\partial w}{\partial \alpha_2}\right)\delta v \\ &+ \left(\frac{1}{A_1}\frac{\partial u}{\partial \alpha_1} + \frac{v}{A_1 A_2}\frac{\partial A_1}{\partial \alpha_2} + \frac{w}{R_1}\right)\delta w + \left(\frac{1}{A_2}\frac{\partial v}{\partial \alpha_2} + \frac{u}{A_1 A_2}\frac{\partial A_2}{\partial \alpha_1} + \frac{w}{R_2}\right)\delta w\Bigg] \mathrm{d}S_0\end{aligned} \tag{29}$$

with the following definitions for a general thin-walled pipe:

$$\begin{aligned} &\mathrm{d}S_0 = A_1 A_2 \, \mathrm{d}\alpha_1 \, \mathrm{d}\alpha_2 \\ &A_1 = R - a\cos\varphi, \quad A_2 = a \\ &\alpha_1 = \theta, \quad \alpha_2 = \varphi \\ &\frac{1}{R_1} = -\frac{\cos\varphi}{R - a\cos\varphi}, \quad \frac{1}{R_2} = \frac{1}{a} \end{aligned} \tag{30}$$

Finally, (29) may be written as follows:

$$W_{ep}^{\mathrm{nl}} = -\int_{S_0} \frac{p}{2a}\left[\frac{au}{R - a\cos\varphi}\left(2\frac{\partial w}{\partial\theta} + u\cos\varphi\right) + v\left(2\frac{\partial w}{\partial\varphi} - v\right) - \frac{R - 2a\cos\varphi}{R - a\cos\varphi}w^2\right]\mathrm{d}S_0 \quad (31a)$$

with

$$\mathrm{d}S_0 = a(R - a\cos\varphi)\,\mathrm{d}\varphi\,\mathrm{d}\theta \quad (31b)$$

Using the displacement model (4)–(6), we can represent the linear part of the pressure work (28) as

$$W_{ep}^{\mathrm{l}} = \int_{S_0} pw\,\mathrm{d}S_0 = \mathbf{g}_p^{\mathrm{T}}\mathbf{q} \quad (32)$$

where $\mathbf{g}_p$ is the nodal loading vector due to the pressure and is defined by the relation

$$\mathbf{g}_p = \sum_e \mathbf{L}_e^{-1}\mathbf{g}_{ep} \quad (33)$$

$$\mathbf{g}_{ep} = \int_{S_e} p[H_k \;\; H_k\cos\varphi \;\; 0 \;\; h_k \;\; h_k\cos\varphi \;\; 0]_k^{\mathrm{T}}\,\mathrm{d}S_0, \quad k = 1,2 \quad (34)$$

$$\mathbf{L}_e\mathbf{q} = \mathbf{q}_e \quad (35)$$

$$\mathbf{q}_e = [(w_0^{\mathrm{s}})_k \;\; (w_1^{\mathrm{s}})_k \;\; (w_1^{\mathrm{a}})_k \;\; [(w_{,r})_0^{\mathrm{s}}]_k \;\; [(w_{,r})_1^{\mathrm{s}}]_k \;\; [(w_{,r})_1^{\mathrm{a}}]_k]_k^{\mathrm{T}}, \quad k = 1,2 \quad (36)$$

where only the related components of $\mathbf{g}_{ep}$ and $\mathbf{q}_e$ are presented.

For the non-linear part of the pressure work (31), we define the following relations:

$$\mathbf{N}_1^{\mathrm{T}}\mathbf{q}_e = \frac{au}{R - a\cos\varphi}, \quad \mathbf{N}_2^{\mathrm{T}}\mathbf{q}_e = 2\frac{\partial w}{\partial\theta} + u\cos\varphi$$

$$\mathbf{N}_3^{\mathrm{T}}\mathbf{q}_e = v, \quad \mathbf{N}_4^{\mathrm{T}}\mathbf{q}_e = 2\frac{\partial w}{\partial\varphi} - v$$

$$\mathbf{N}_5^{\mathrm{T}}\mathbf{q}_e = w, \quad \mathbf{N}_6^{\mathrm{T}}\mathbf{q}_e = -\frac{R - 2a\cos\varphi}{R - a\cos\varphi}w \quad (37)$$

where $\mathbf{N}_i$ is the coefficient vector of the generalized nodal displacement components [8]. Therefore, the non-linear component of the pressure work can be presented as follows:

$$W_{ep}^{\mathrm{nl}} = -\sum_e \int_{S_e} \frac{p}{2a}[\mathbf{q}_e^{\mathrm{T}}\mathbf{N}_1\mathbf{N}_2^{\mathrm{T}}\mathbf{q}_e + \mathbf{q}_e^{\mathrm{T}}\mathbf{N}_3\mathbf{N}_4^{\mathrm{T}}\mathbf{q}_e + \mathbf{q}_e^{\mathrm{T}}\mathbf{N}_5\mathbf{N}_6^{\mathrm{T}}\mathbf{q}_e]\,\mathrm{d}S_0 \quad (38)$$

We define a stiffness matrix $\mathbf{K}_p$ as

$$\mathbf{K}_p = \sum_e (\mathbf{L}_e)^{\mathrm{T}}\mathbf{K}_{ep}\mathbf{L}_e \quad (39)$$

with

$$\mathbf{K}_{ep} = \int_{S_e} \frac{p}{a}[\mathbf{N}_1\mathbf{N}_2^{\mathrm{T}} + \mathbf{N}_3\mathbf{N}_4^{\mathrm{T}} + \mathbf{N}_5\mathbf{N}_6^{\mathrm{T}}]\,\mathrm{d}S_0 \quad (40)$$

$\mathbf{K}_p$ corresponds to the effect of restitution of internal pressure. So (38) becomes

$$W_{ep}^{\mathrm{nl}} = -\tfrac{1}{2}\,\mathbf{q}^{\mathrm{T}}\mathbf{K}_p\mathbf{q} \tag{41}$$

However, it should be pointed out that $\mathbf{K}_{ep}$ defined in (40) (and also $\mathbf{K}_p$ in (39)) is a non-symmetric matrix. In order to use standard finite element method, we proceed a matrix decomposition that produces two separated matrices:

$$\mathbf{K}_p = \mathbf{K}_p^{\mathrm{s}} + \mathbf{K}_p^{\mathrm{a}} \tag{42}$$

Supposing that k_{ij} is the components of matrix $\mathbf{K}_p$, we define

$$\mathbf{K}_p^{\ell} = \begin{bmatrix} k_{11}^{\mathrm{l}} & k_{12}^{\mathrm{l}} & \cdots & k_{1n}^{\mathrm{l}} \\ k_{21}^{\mathrm{l}} & k_{22}^{\mathrm{l}} & \cdots & k_{2n}^{\mathrm{l}} \\ \vdots & \vdots & & \vdots \\ k_{n1}^{\mathrm{l}} & k_{n2}^{\mathrm{l}} & \cdots & k_{nn}^{\mathrm{l}} \end{bmatrix} \tag{43}$$

where

$$l = \mathrm{s}\ (\text{symmetric}) \quad k_{ij}^{\mathrm{s}} = \tfrac{1}{2}(k_{ij} + k_{ji}), \quad k_{ij}^{\mathrm{s}} = k_{ji}^{\mathrm{s}} \tag{44}$$

$$l = \mathrm{a}\ (\text{anti-symmetric}) \quad k_{ij}^{\mathrm{a}} = \tfrac{1}{2}(k_{ij} - k_{ji}), \quad k_{ij}^{\mathrm{a}} = -\,k_{ji}^{\mathrm{a}} \tag{45}$$

So we obtain a symmetric matrix $\mathbf{K}_p^{\mathrm{s}}$ and an anti-symmetric matrix $\mathbf{K}_p^{\mathrm{a}}$. By the following relations,

$$\mathbf{q}^{\mathrm{T}}\mathbf{K}_p^{\mathrm{a}}\mathbf{q} = \sum_{i=1}^{n}\sum_{j=1}^{n} q_i q_j k_{ij}^{\mathrm{a}} = \sum_{i=1}^{n}\sum_{j=1}^{n} \tfrac{1}{2} q_i q_j (k_{ij}^{\mathrm{a}} + k_{ji}^{\mathrm{a}}) = 0 \tag{46a}$$

$$\mathbf{q}^{\mathrm{T}}\mathbf{K}_p^{\mathrm{s}}\mathbf{q} = \sum_{i=1}^{n}\sum_{j=1}^{n} q_i q_j k_{ij}^{\mathrm{s}} = \sum_{i=1}^{n}\sum_{j=1}^{n} \tfrac{1}{2} q_i q_j (k_{ij}^{\mathrm{s}} + k_{ji}^{\mathrm{s}}) = \mathbf{q}^{\mathrm{T}}\mathbf{K}_p\mathbf{q} \tag{46b}$$

we have verified that $\mathbf{K}_p^{\mathrm{s}}$ obtained by (43) and (44), which is symmetric and will be used in (41), is equivalent to $\mathbf{K}_p$.

On the other hand, Almeida [5] has also proposed a formulation for pipe element to consider the stiffening effect of internal pressure although the used displacement model (7) does not allow him to consider the extension effect of pressure. By means of pressure-work mapping, he arrived at the following result:

$$W_p^{\mathrm{nl}} = \frac{-p}{8}\int_{-1}^{+1}\int_{0}^{2\pi}\left[v^2 - \left(\frac{\mathrm{d}^2 v}{\mathrm{d}\varphi^2}\right)^2\right](R - a\cos\varphi)\theta\,\mathrm{d}\varphi\,\mathrm{d}r \tag{47}$$

By a similar procedure as above, he obtained the complementary stiffness matrix:

$$\mathbf{K}_{ep} = \frac{p}{4}\int_{-1}^{+1}\int_{0}^{2\pi}[\mathbf{Q}_1\mathbf{Q}_1^{\mathrm{T}} - \mathbf{Q}_2\mathbf{Q}_2^{\mathrm{T}}](R - a\cos\varphi)\theta\,\mathrm{d}\varphi\,\mathrm{d}r \tag{48}$$

where the definition below is used:

$$\mathbf{Q}_1\mathbf{q}_e^{\mathrm{T}} = v, \quad \mathbf{Q}_2\mathbf{q}_e^{\mathrm{T}} = \frac{\mathrm{d}^2 v}{\mathrm{d}\varphi^2} \tag{49}$$

The formulation of Almeida [5] is still applicable for the present enhanced elbow element by supposing that the restitution effect of pressure concerns only the ovalization v^c and this effect is only related to the inextensible part of the hoop strain. The numerical comparison will be presented in Section 5.2.

Now let us suppose that the pipe elbow is subjected to internal pressure p and other general loading. The virtual work principle is written as

$$\delta W_{\text{in}} = \delta(W_{\text{ex}} + W_{ep}^{\text{l}} + W_{ep}^{\text{nl}}) \tag{50}$$

where W_{in} is the internal virtual strain energy, W_{ep}^{l} and W_{ep}^{nl} represent respectively the linear and non-linear parts of virtual work of the pressure and W_{ex} is the external virtual work of other loading. Using (21), (22), (32) and (41), we obtain the equilibrium equation of the structure:

$$[\mathbf{K} + \mathbf{K}_p]\mathbf{q} = \mathbf{g} + \mathbf{g}_p \tag{51}$$

where the matrix $\mathbf{K}_p$, defined in (39), represents the restitution effect of the internal pressure.

3.2. Axial force effect of internal pressure in an end-closed elbow

As stated before, the developed pipe elbow element is a beam model enhanced by Fourier series to describe the shell behaviour. The geometry of the element is represented by the curved axis of the elbow. As a consequence, the area difference between the intrados and extrados parts of a curved pipe, which will lead to non-uniform hoop stress, is not yet considered. On the other hand, for an end-closed curved pipe, the self-equilibrium relation between internal pressure and axial force due to the pressure is not represented by the element formulation. These two shortcomings will be overcome by simple numerical techniques.

Considering a part of a curved pipe subjected to uniform internal pressure, the area difference between the intrados and extrados parts will cause a radial load component p^*, which could be supposed to apply on the axis line of curved pipe, see Figure 4.

Take an infinitesimal surface on pipe at circular angle φ:

$$\mathrm{d}S = a(R - a\cos\varphi)\,\mathrm{d}\varphi\,\mathrm{d}\theta \tag{52}$$

Its mean value corresponding to $\varphi = 90^\circ$ is

$$\overline{\mathrm{d}S} = aR\,\mathrm{d}\varphi\,\mathrm{d}\theta \tag{53}$$

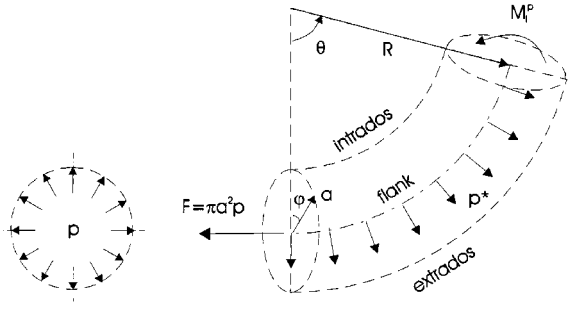

Figure 4. Equilibrium between internal pressure and axial force for an end-closed curved pipe

The relative difference between (52) and (53) can be represented by the following formula:

$$\frac{\Delta(\mathrm{d}S)}{\overline{\mathrm{d}S}} = -\frac{a}{R}\cos\varphi \tag{54}$$

So a fictitious centrifugal force (along the direction from intrados to extrados) due to (54) can be calculated for a unit of axial length of the curved pipe ($\mathrm{d}\theta = 1/R$):

$$p^* = 4\int_0^{\pi/2} p\,\frac{a^2}{R}\cos^2\varphi\,\mathrm{d}\varphi = \frac{a^2\pi}{R}\,p \tag{55}$$

This force may be considered to apply on the axis line of the curved pipe for the present pipe elements. For an end-closed curved pipe, the axial force due to internal pressure is

$$F_0 = \pi a^2 p \tag{56}$$

From Figure 4, we can calculate the bending moment at any section due to internal pressure and its corresponding end force as

$$\begin{aligned} M_{\mathrm{I}}^p &= F_0(1-\cos\theta)R - 2p^*R^2\sin^2(\theta/2) \\ &= \pi a^2 pR(1-\cos\theta) - 2\pi a^2 pR\sin^2(\theta/2) = 0 \end{aligned}$$

We note that although the internal bending moment is null at any cross-section the rotation at any section may be not zero. In fact, the internal pressure has a small effect of opening the curved pipe. In order to consider the effect of axial force due to the internal pressure, we employ an approximate method. We apply the fictitious pressure p^* by (55) on axis line of curved pipe, which is transmitted into corresponding beam d.o.f. of pipe element. The additional loading vector due to this effect can be calculated as

$$\mathbf{g}_{\mathrm{b}} = \sum_e \mathbf{L}_e^{-1}\mathbf{g}_{\mathrm{b}p} \tag{57a}$$

$$\mathbf{g}_{\mathrm{b}p} = \int_{\Gamma_e} \frac{a^2 p}{R}\{0 \;\; L_k\cos\theta \;\; -L_k\sin\theta \;\; 0 \;\; 0 \;\; 0\}_k^{\mathrm{T}}\,\mathrm{d}\Gamma, \quad k = 1,4 \tag{57b}$$

where Γ_e is the element length (axis line of curved pipe) and L_k is k-node interpolation function. The integral of (57b) can be dealt with analytically or numerically.

3.3. The weakening effect due to non-uniformity of hoop stress of curved pipe under internal pressure

It is well known that for a straight pipe under internal pressure, stresses and strains are axisymmetric. However, for a curved pipe, as it is discussed above, the area difference between the intrados and extrados parts of curved pipe will result in non-axisymmetry of stresses. This situation decreases the capacity of bearing pressure of a curved pipe.

Figure 5(a) illustrates the force by (55) due to internal pressure (in direction from intrados to extrados, denoted here as $-z$ direction) should be in equilibrium with the z-component of axial force F_0:

$$2F_0\sin\left(\frac{\Delta\theta}{2}\right) = p^*R\Delta\theta \tag{58}$$

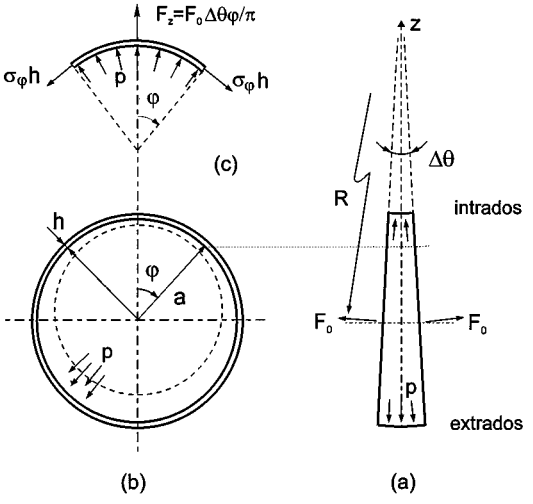

Figure 5. Static equilibrium of curved pipe under internal pressure

By taking $\Delta\theta$ as small enough and by using (55), we obtain again $F_0 = \pi a^2 p$ as (56). Now we take out one part of pipe shell as Figure 5(c) and consider the static equilibrium in the z direction:

$$\sigma_\varphi h \Delta\theta (R - a\cos\varphi)\sin\varphi = F_0 \Delta\theta \frac{\varphi}{\pi} + \int_0^\varphi p\Delta\theta (R - a\cos\varphi)\cos\varphi a \, \mathrm{d}\varphi \tag{59}$$

we obtain finally

$$\sigma_\varphi = \frac{pa}{h}\frac{2R - a\cos\varphi}{2(R - a\cos\varphi)} = C_1 \bar{\sigma}_\varphi \tag{60}$$

where

$$C_1 = \frac{2R - a\cos\varphi}{2(R - a\cos\varphi)}, \quad \bar{\sigma}_\varphi = \frac{pa}{h} \tag{61}$$

C_1 is a stress index representing the ratio of the hoop stress at point φ of curved pipe section and the mean stress of a straight pipe. In another way, we can represent the hoop stress by two components, one is the mean corresponding to a straight pipe and the other its difference along the circumference (φ):

$$\sigma_\varphi = \bar{\sigma}_\varphi + \Delta\sigma_\varphi \tag{62}$$

$$\Delta\sigma_\varphi = \frac{pa}{h}\frac{a\cos\varphi}{2(R - a\cos\varphi)} \tag{63}$$

The maximum of $\Delta\sigma_\varphi$ and σ_φ is attained at the intrados of the curved pipe:

$$\Delta\sigma_{\varphi_{\max}} = \frac{a^2 p}{2h(R - a)} \tag{64}$$

$$\sigma_{\varphi_{\max}} = \frac{pa}{h}\frac{2R - a}{2(R - a)} \tag{65}$$

From (65), we may easily deduce the analytical solution for the plastic collapse limit load for a thin-walled curved pipe under internal pressure (without the effect of axial stress):

$$p_l = \frac{1 - a/R}{1 - a/2R} \frac{\sigma_y h}{a} \tag{66}$$

where σ_y is yield limit of the material. This solution identifies to that of Goodall [10], who obtained it by resolving the differential equations of thin shell. When $a/R \to 0$, we get the limit pressure solution of a thin-walled straight pipe:

$$p_l^o = \frac{\sigma_y h}{a} \tag{67}$$

The non-uniformity of hoop stress stated as above may be simulated by the present elbow element owing to the development in Section 2, where we have introduced new terms into the radial displacement model to describe the non-symmetric deformation. For a slightly curved pipe, equation (63) may be approximated as

$$\Delta\sigma_\varphi \to \frac{pa}{h} f(a/R) \cos\varphi \tag{68}$$

This could be described by the in-plane non-symmetric term $w_1^s \cos\varphi$ in (6). However for a highly curved pipe with $a/R \to 1$, some harmonic terms of higher order such as $\sum w_m^s \cos m\varphi$, $m = 1, 3, 5 \ldots$, are needed to describe accurately the theoretical stress field. It is not difficult to insert these terms but it will increase the computing cost. In this paper, two simple and effective approaches are proposed for using only the model $w_1^s \cos\varphi$ to simulate real hoop stress distribution (62), (63).

Model 1: *Maximum stress model.* The hoop stress at the intrados of curved pipe is defined as same to that given by (65), because this stress determines mainly the plastic collapse limit of internal pressure. The variation of the hoop stress is represented as (69). The additional nodal load vector relative to (34) can be calculated by (70)

$$\Delta\sigma_\varphi \to \frac{pa}{h} \frac{a/R}{2(1 - a/R)} \cos\varphi \tag{69}$$

$$\mathbf{g}_{ewp}^{\mathrm{I}} = \int_{S_e} \frac{a/R}{2(1 - a/R)} p \, [0 \;\; H_k \;\; 0 \;\; 0 \;\; h_k \;\; 0]_k^{\mathrm{T}} \, \mathrm{d}S_0, \quad k = 1, 2 \tag{70}$$

This model is compared with the analytic stress field in Figure 6. We see that the stress in the intrados part of curved pipe is well simulated, but it increases the stress variation between the intrados and the extrados.

Model 2: *Modified maximum stress model.* As model 1, the maximum hoop stress at intrados is simulated, but the maximum variation of hoop stress is also simulated by (71). This is realized by using (72) to calculate the additional nodal loading vector relative to (34):

$$\Delta\sigma_\varphi \to \frac{pa}{h} \frac{a/R}{2(1 - a^2/R^2)} \cos\varphi \tag{71}$$

$$\mathbf{g}_{epw}^{\mathrm{II}} = \int_{S_e} \frac{a/R}{2(1 - a^2/R^2)} p \left[\frac{a}{R} H_k \;\; H_k \;\; 0 \;\; \frac{a}{R} h_k \;\; h_k \;\; 0 \right]_k^{\mathrm{T}} \mathrm{d}S_0, \quad k = 1, 2 \tag{72}$$

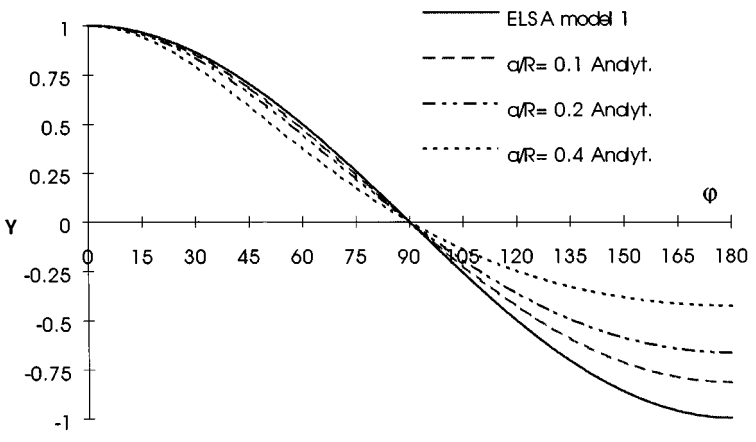

Figure 6. Hoop stress distribution by model I

$$\left(Y = \Delta\sigma_{\varphi}\frac{h}{pa}\frac{2(1-a/R)}{a/R}\right)$$

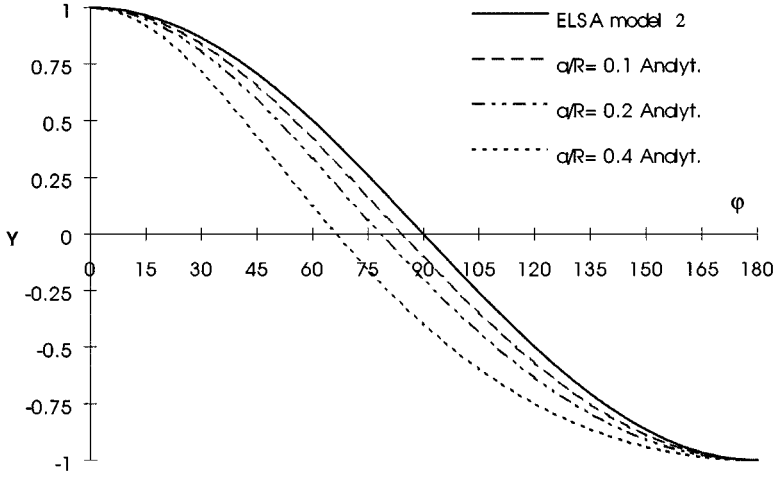

Figure 7. Hoop stress distribution by model 2

$$\left(Y = \Delta\sigma_{\varphi}\left[1+\frac{a^2/R^2}{2(1-a^2/R^2)}\right]\frac{h}{pa}\frac{2(1-a^2/R^2)}{a/R}\right)$$

We see in Figure 7 that the hoop stress is well simulated at the parts of intrados and extrados but overestimated a little at the flank of the curved pipe.

Numerical comparison of plastic limit analysis by above two computing models with analytical solutions will be presented in Section 5.3.

4. KINEMATIC FORMULATION OF PLASTIC LIMIT ANALYSIS

One of the principal objectives of developing pipe elbow element in this paper is to find the plastic limit load of pipe structures by kinematic mathematical programming method. Due to the fact that plastic analysis of a pipe elbow structure is much more complicated and expensive than a usual elastic analysis, the use of simple but effective pipe elements is very interesting. We formulate here only some principal points for the present application neglecting the theoretical details [8]. Starting from Markov variational principle, cf. [4], one can deduce a so-called kinematic (upper bound) theorem stated as following:

For a structure consisting of an ideal plastic material, the actual limit load multiplier α *of the structure is the smallest one of the set of multipliers* α^+ *corresponding to any kinematically admissible and incompressible velocity field* $\dot{\mathbf{u}}$:

$$\alpha = \min \alpha^+, \quad \alpha^+ = W_i \tag{73a}$$

$$\text{s. t. } W_e = 1 \tag{73b}$$

W_i and W_e are, respectively, the internal dissipated and external loading power defined as below:

$$W_i = \int_V D(\dot{\boldsymbol{\varepsilon}})\, \mathrm{d}V = \int_V \frac{2}{\sqrt{3}}\, \sigma_y J_2^{1/2}(\dot{\boldsymbol{\varepsilon}})\, \mathrm{d}V \tag{74}$$

$$W_e = \int_V \mathbf{f}_0^{\mathrm{T}} \dot{\mathbf{u}}\, \mathrm{d}V + \int_{S_t} \mathbf{t}_0^{\mathrm{T}} \dot{\mathbf{u}}\, \mathrm{d}S \geqslant 0 \tag{75}$$

$$\dot{\boldsymbol{\varepsilon}} = \nabla \dot{\mathbf{u}} \tag{76}$$

where σ_y is the yield limit of the material, J_2 is the second invariant of the strain rate that will be defined later.

It is defined in (73a) that $\alpha = \mathbf{P}_l / \mathbf{P}_0$, where $\mathbf{P}_l = (\mathbf{f}_l, \mathbf{t}_l)$ and $\mathbf{P}_0 = (\mathbf{f}_0, \mathbf{t}_0)$ are respectively the plastic limit load and the chosen reference load. Here we have supposed that all loads are applied in a monotonic and proportional way. Therefore, the calculation of limit load becomes a minimization procedure. To resolve it, the method of the reduced-gradient algorithm in conjunction with a quasi-Newton algorithm is used [11].

In the present work concerning the pipe structures, the kinematically admissible field required by the programming formulation of (73)–(76) is provided by using the enhanced elbow elements presented in Sections 2 and 3. Using the hypotheses of Kirchhoff–Love, the stress normal to the surface of a thin pipe is neglected. As a consequence, we could write relation (77) for a rigid-perfectly plastic material [8]. We note that this material model gives a limit load solution same as an elastic-perfectly plastic material:

$$\dot{\varepsilon}_\zeta = -(\dot{\varepsilon}_\eta + \dot{\varepsilon}_\xi) \tag{77}$$

It means that the condition of incompressibility could be satisfied. The second invariant of strain rate deviator becomes

$$J_2 = \frac{1}{2}\, \dot{\varepsilon}_{ij}\, \dot{\varepsilon}_{ij} = \dot{\varepsilon}_\eta^2 + \dot{\varepsilon}_\xi^2 + \dot{\varepsilon}_\eta^2 \dot{\varepsilon}_\xi^2 + \frac{\dot{\gamma}_{\eta\xi}^2}{4} + \frac{\dot{\gamma}_{\eta\zeta}^2}{4} \tag{78}$$

or in matrix form

$$J_2(\dot{\boldsymbol{\varepsilon}}) = \dot{\boldsymbol{\varepsilon}}^{\mathrm{T}} \bar{\mathbf{D}}_p \dot{\boldsymbol{\varepsilon}} = \dot{\mathbf{q}}_e^{\mathrm{T}} \mathbf{B}^{\mathrm{T}} \bar{\mathbf{D}}_p \mathbf{B} \dot{\mathbf{q}}_e \tag{79a}$$

with

$$\bar{\mathbf{D}}_p = \begin{bmatrix} 1 & 0 & 0 & 1/2 \\ 0 & 1/4 & 0 & 0 \\ 0 & 0 & 1/4 & 0 \\ 1/2 & 0 & 0 & 1 \end{bmatrix} \tag{79b}$$

Therefore, (74) and (75) can be written in the following matrix form by assembling over all elements of the structure:

$$W_i = \sum_e \frac{2\sigma_y}{\sqrt{3}} \int_{V_e} [(\mathbf{B}\dot{\mathbf{q}}_e)^{\mathrm{T}} \bar{\mathbf{D}}_p \mathbf{B} \dot{\mathbf{q}}_e]^{1/2} \tag{80}$$

$$W_e = \sum_e \left[\int_{V_e} (\mathbf{N}\dot{\mathbf{q}}_e)^{\mathrm{T}} \bar{\mathbf{f}}_0 \, \mathrm{d}V + \int_{S_e} (\mathbf{N}\dot{\mathbf{q}}_e)^{\mathrm{T}} \mathbf{t}_0 \, \mathrm{d}S \right] = \mathbf{g}^{\mathrm{T}} \dot{\mathbf{q}} \tag{81}$$

$$\dot{\mathbf{q}}_e = \mathbf{L}_e \dot{\mathbf{q}}, \quad \mathbf{g} = \sum_e \mathbf{L}_e \mathbf{g}_e \tag{82}$$

where $\dot{\mathbf{q}}$ and $\mathbf{g}$ are respectively the global node-displacement rate vector and the corresponding load vector and $\mathbf{L}_e$ is the matrix of localization.

It is necessary to point out that by using a general (solid) displacement finite element the incompressibility condition may not be satisfied. In this case, a so-called modified Markov variational principle proposed in [8] may be used. Further limit analysis of cracked structures has be presented in [12], and shakedown analysis with varying loads including thermal loading in [13].

5. APPLICATION

The improved elbow element has been implemented in the computing program ELSA (Elbow and structure – Limit and Shakedown Analysis) developed in our laboratory. In this paper, we present two elastic sample analyses and some applications in plastic limit analysis.

5.1. Displacement modelling of cylindrical shell under bending

For the sake of numerical examination, we study the deformation of a straight pipe (one end of the pipe is fixed and the other is under bending) with the following computing data (cf. Figure 3): $L = 15$ m, $r_{\mathrm{m}} = 5$ m, $h = 0{\cdot}05$ m, $E = 2{\cdot}1 \times 10^5$ MPa, $v = 0{\cdot}3$, $M = 2{\cdot}985 \times 10^5$ kNm.

The results are obtained respectively by SAMCEF (a commercial finite element software) using 576 shell elements with 2021 nodes, and by ELSA using four enhanced pipe elements with 13 nodes. We compare at first the displacement along line AB (of Figure 3) in the x-direction (u) and z-direction (w) in Figure 8, where a simplified analytic solution of Xue [14] is also marked for comparison.

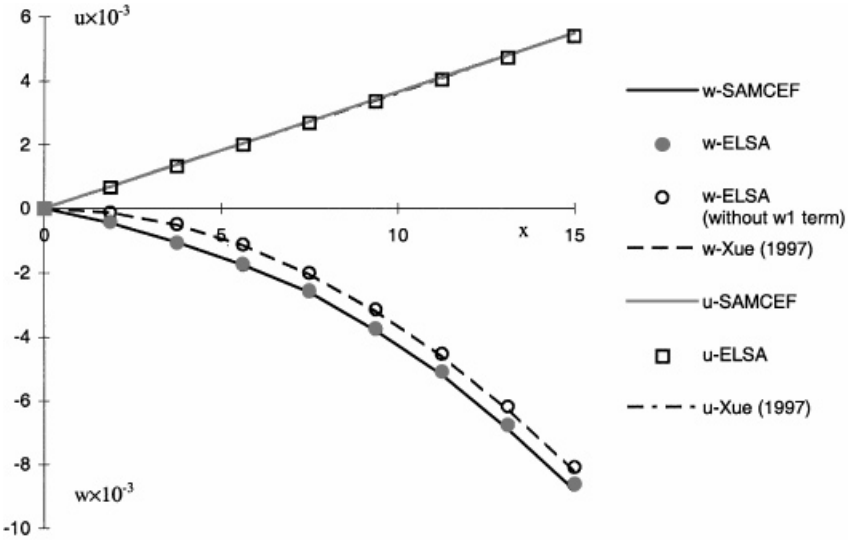

Figure 8. Comparison of deformation of pipe along line AB of Figure 3

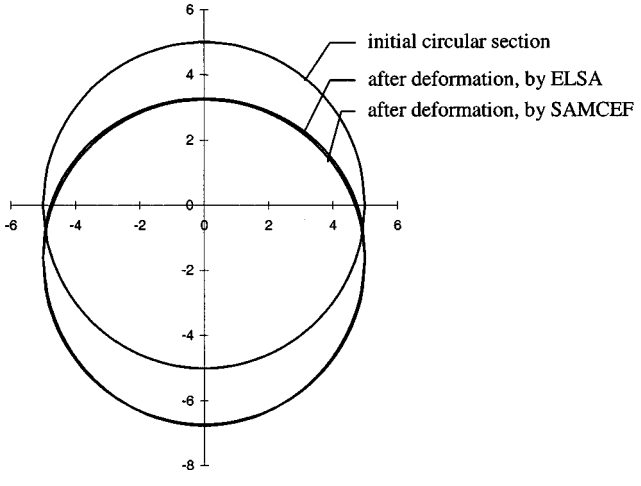

Figure 9. Deformation prediction of loading section by ELSA and SAMCEF

It is clearly shown that the results of axial displacement (u) by the three methods are identical. For z-direction, displacement (w), the present solutions (ELSA) with a new displacement model considering non-symmetrical deformation are in excellent agreement with that of SAMCEF. This justifies the proposed displacement model. On the other hand, it is interesting to notice that if we do not consider the non-symmetric deformation W_1^s, the solution of ELSA coincides with that of Xue [14]. This means that the analytic solution of Xue is only an approximation to the real solution. Now we consider the deformation of section B (cf. Figure 3), it is clearly seen in Figure 9 that the prediction by the present pipe element agrees well with that of SAMCEF although the numbers of used elements and the computing cost are so different.

5.2. *The effect of internal pressure on flexibility factor of curved pipe*

A 90° elbow connected to two straight pipes at the two ends of the elbow is subjected to in-plane traversal loading. It is well known that a curved pipe under bending is more flexible than that would be predicted by the elementary beam theory due to ovalization and warping of the pipe section. This characteristic of curved pipe is recognized in the pipe flexibility calculation by use of 'flexibility factor' k_f that is simply the ratio of the actual flexibility to that predicted by the elementary beam theory. According to von Karman's theoretical solution, the flexibility factor k_f is given by the formula

$$k_f = \frac{1{\cdot}65}{\lambda} \geqslant 1 \tag{83}$$

where

$$\lambda = \frac{Rh}{a^2} \tag{84}$$

However as discussed in Section 3.1, internal pressure has the effect to increase the stiffness of curved pipes so it will decrease the flexibility factor k_f for a thin curved pipe. The geometry and loading are shown in Figure 10, where one-half of the structure is discretized by five enhanced pipe elements with 16 nodes. The obtained results, in Figure 11, are compared with the experimental results of Rodabaugh and Geoge [15] and the numerical ones of Almeida [5]. It is shown that the flexibility factor k_f indeed decreases with the increase of internal pressure.

5.3. *Plastic limit of cylindrical pipe under bending (cf. Figure 3)*

Now we calculate the plastic limit of structures by using the enhanced pipe elbow element and the direct programming method. Here we consider at first a straight pipe without the end effect,

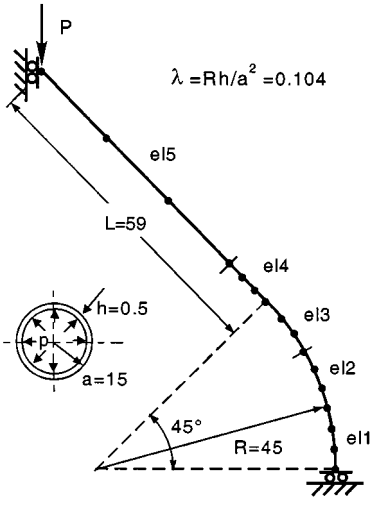

Figure 10. Curved pipe to bending and internal pressure

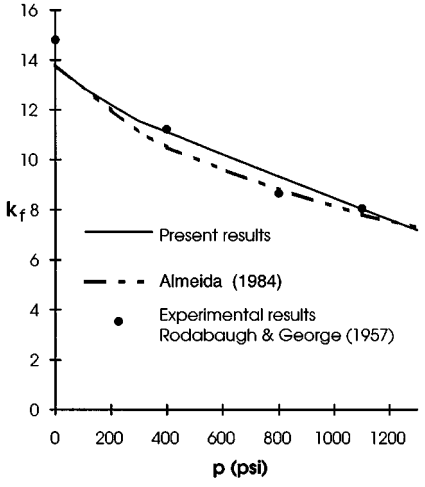

Figure 11. Effect of internal pressure on flexibility factor

Table I. Limit factor of bending moment α_l of straight pipe, $\alpha_l = M/M_l$

Method	Property of solution	Num. of elem.	Integration points†	α_l	Used elements
Analytic solution	Exact	—	—	1·000	—
ELSA software	Upper bound	3	$3 \times 14 \times 4$	1.002	Enhanced elbow element
		3	$3 \times 14 \times 4$	1·158	Bathe–Militello elbow element

† Numerical integration order $l \times m \times n$. l: axial, m: circular, n: radial (thickness)

because its analytic solution of plastic limit may be obtained by the elementary beam theory:

$$M_l = 4\sigma_y h\left(r^2 + \frac{h^2}{12}\right) \tag{85}$$

We see in Table I for the limit bending moment that there is an error of 15·8 per cent in using the Bathe–Militello element, while an excellent solution is obtained with the present enhanced element. It is useful to explain this important improvement. It has been pointed out in Section 2.2 that the Bathe–Militello element has no parameter representing the non-symmetric deformation shown in Figure 3. This leads to such a consequence that the hoop membranous strain must vanish. According to plastic normality rule,

$$\dot{\varepsilon}_{ij}^{\mathrm{p}} = \dot{\lambda}\frac{\partial f}{\partial \sigma_{ij}} \quad \text{with} \quad \dot{\lambda} \geqslant 0 \tag{86}$$

where $\dot{\lambda}$ is a plastic multiplier and f is von Mises' yield function

$$f = \sqrt{\sigma_\varphi^2 + \sigma_x^2 - \sigma_\varphi \sigma_x} - \sigma_y = \sigma_{\mathrm{eq}} - \sigma_y \tag{87}$$

we have

$$\dot{\varepsilon}_{\theta}^{\mathrm{p}} = \dot{\lambda}\,\frac{2\sigma_{\varphi} - \sigma_{x}}{\sigma_{\mathrm{eq}}} \tag{88}$$

Since $\dot{\varepsilon}_{\varphi}^{\mathrm{p}}$ must vanish with the displacement model of the Bathe–Militello element, one has

$$\sigma_{\varphi} = \sigma_{x}/2$$

Substituting this result into (87), we obtain $\sigma_x = 2/\sqrt{3}\sigma_{\mathrm{y}}$. Taking M_l (or σ_{y}) as reference, the limit factor becomes

$$\alpha_l = \sigma_x/\sigma_y = 1{\cdot}1547$$

This explains the difference of the results (about 15·5 per cent) obtained by using the present element and the Bathe–Militello element in the case of non-symmetric loading. On the other hand, with our improvement, the non-symmetric deformation may be well modelled and excellent results may be obtained in both elastic and plastic calculation.

5.4. Plastic limit of 90° elbow under internal pressure

We consider a curved pipe as a torus under internal pressure to verify the numerical models proposed in Section 3.3 for the simulation of the non-uniformity of hoop stress. Two elements with seven nodes are used. The results of limit pressure are shown in Table II, where both analytic and numerical solutions do not include the effect of axial forces. It appears that the proposed models 1 and 2 are nearly equivalent and give good predictions in comparison with analytic solutions. However, for a highly curved pipe, the present results may be a lower bound due to the approximation of the proposed models.

5.5. Plastic limit of 90° elbow subjected to in-plane bending

A curved pipe (elbow) is subjected to bending moment M_1 in its symmetric plane. The end effect is not included because the analytic solution is known in this case. Calladine [16] proposed a so-called lower bound solution (89a) for a highly curved pipe. This solution was supported by much theoretical and experimental work in literature and was considered as a good approximation of the exact solution. For a slightly curved pipe ($\lambda > 0{\cdot}7$), equation (89b) is proposed by Yan in [8, 17]. Hence, equation (89) constructs a complete solution of in-plane elbow of all geometry

Table II. Plastic limit pressure of curved pipe $\alpha_l^p = p_l/p_l^0$, p_l^0: (67)

		Numerical solution		Analytical solution
a/R	λ (84)	Model 1(70)	Model 2 (72)	(66)
0·221	0·903	0·881	0·881	0·875
0·4	0·5	0·749	0·751	0·750
0·551	0·363	0·600	0·609	0·620

Note: Mean radius $a = 300$ mm and thickness $h = 60$ mm.

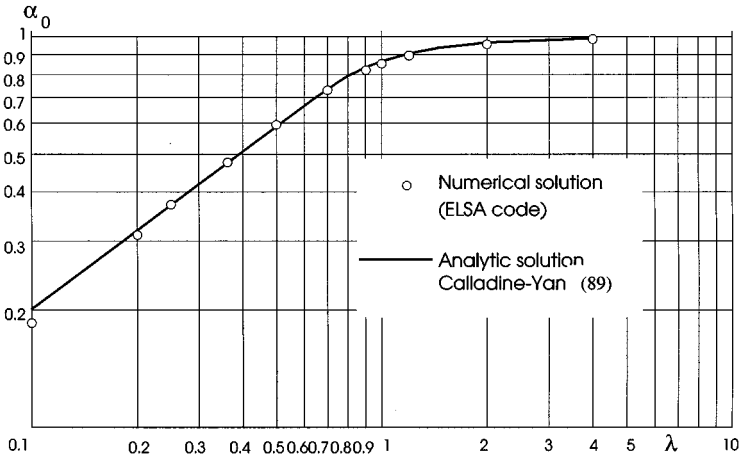

Figure 12. Limit factor of in-plane bending moment of elbow: $\alpha = M_l/M_I$

with free end condition (torus):

$$\alpha_0 = 0{\cdot}9346\lambda^{2/3} \quad \text{for } \lambda < 0{\cdot}7 \tag{89a}$$

$$\alpha_0 = \cos\left(\frac{\pi}{6\lambda}\right) \quad \text{for } \lambda \geqslant 0{\cdot}7 \tag{89b}$$

where λ is defined by (84) and we define

$$\alpha_0 = M_l/M_I \tag{89c}$$

with M_l being the in-plane limit moment of the curved pipe and M_I the straight pipe solution (85) as reference. From Figure 12, we obtain excellent agreement between analytic and numerical solutions for all λ values.

5.6. Pipe elbow structure under complex loading (*in-plane and out-of-plane bending, internal pressure and axial force*)

As the last example, we consider plastic limit solution of a pipe elbow structure under complex loading as shown in Figure 13. Different combinations of loading are dealt with. The in-plane bending moment is in the direction of closing the elbow. It will be very expensive to solve this problem by a traditional elastic–plastic calculation using three-dimensional or shell elements. However, as shown in Figure 14, using the present direct programming method with a few enhanced elbow elements, satisfactory solutions are obtained. Typically, only nine enhanced elbow elements are used for whole structure (five for elbow and two for each straight pipe), or five elements for one-half of structure if out-of-plane bending moment M_{II} is absent. We note that in Figure 14, M and M_o are respectively the plastic limit moment with and without internal pressure p (and F); p_l is given by (66). The details of the numerical calculation and the deduction of analytic solution are presented in [8, 17].

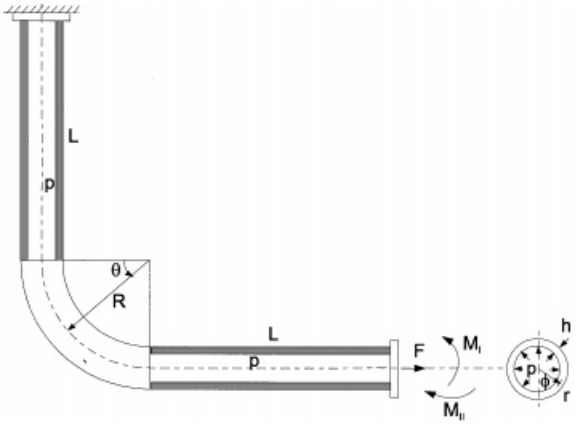

Figure 13. Elbow with prolongation under combined loading (in-plane and out-of-plane bending, pressure, and axial force)

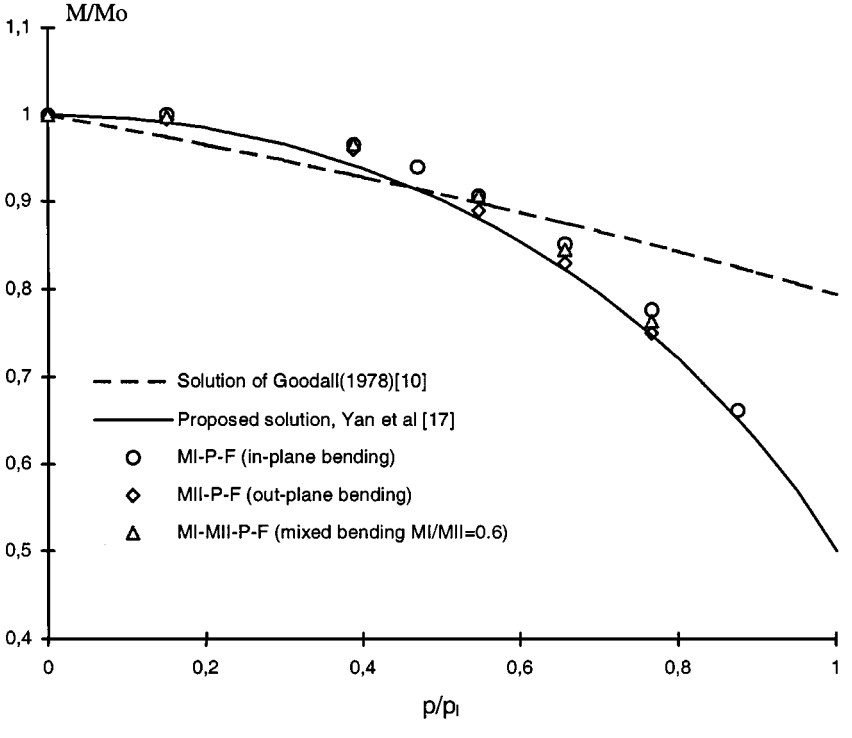

Figure 14. Interaction solution of general bending and internal pressure of close-ended pipe elbow ($\lambda = 0{\cdot}5$) (M_{I}: in plane bending moment; M_{II}: out-of-plane bending moment; P: internal pressure; F: axial force due to the pressure)

6. CONCLUSION

In this paper, we have presented a new development of the enhanced elbow element formulation on the basis of the previous work of Bathe and Almeida [1] and Militello and Huespe [3]. Some important improvements are reached with a new displacement model and a new numerical method. It extends largely the computing capacity of the element. It is shown in this paper that with a few improved elements, a complex three-dimensional pipe elbow structure under complex loading could be efficiently modelled with a quite low computing cost. This advantage is very important for plastic limit analysis by the direct mathematical programming procedure and also for a general non-linear analysis.

Since the original element formulation does not consider the area difference between the intrados and the extrados of elbow, the non-uniformity of hoop stress due to internal pressure on a curved pipe must be simulated with aid of the fictitious force applying on the non-symmetric radial displacement W_1^s. This has been verified to be a simple and effective method, although the simulation remains an approximation of accurate solution. The numerical examination shows that for general engineering application the present enhanced elbow element and direct programming method seem to have enough precision. Especially, the data preparation is very simple and computing cost is low in comparison with three-dimensional or special shell elements.

REFERENCES

1. Bathe KJ, Almeida CA. A simple and effective pipe elbow element—Linear analysis. *Journal of Applied Mechanics* 1980; **47**:93–100.
2. Bathe KJ, Almeida CA. A simple and effective pipe elbow element—Interaction effects. *Journal of Applied Mechanics* 1982; **49**:165–171.
3. Militello C, Huespe AE. A displacement-based pipe elbow element. *Computers and Structures* 1988; **29**(2):339–343.
4. Washizu K. *Variational Methods in Elasticity and Plasticity* (3rd edn). Pergamon Press: Oxford, 1982.
5. Almeida CA. Efeitos da pressão interna no comportamento geral de tubulações: o elemento viga-tubo. Pontificia Universidade Catolica, RJ, Brezil, 1984.
6. Jospin RJ. Etats limites des tuyauteries par la méthode des éléments finis et la programmation mathématique. *Thèse de doctorat*, Université de Liège, Belgium, 1992.
7. Novozhilov VV. *The Theory of Thin Shells*. P. Noordhoff: Groningen, 1959.
8. Yan AM. Contributions to the direct limit state analysis of plastified and cracked structures. *Doctoral Thesis*, University of Liege, Belgium, 1997.
9. Yan AM, Nguyen DH, Jospin RJ. Internal pressure effects on the limit load of elbows. *Proceedings of International Symposium on Shell and Spatial Structures*, 10–14 November, Singapore, 1997; 911–920.
10. Goodall IM. Lower bound limit analysis of curved tubes loaded by combined internal pressure and in-plane bending moment. CEGB-RD/B/N4360, Central Electricity Generating Board, August 1978.
11. Murtagh BA, Saunders MA. MINOS 5.1 - User's Guide. *Technical Report SOL 83-20R*, Stanford University, 1987.
12. Yan AM, Nguyen DH. Limit analysis of cracked structures using mathematical programming and finite element technique. In *ACOMEN'98—Advanced Computational Methods in Engineering*, Van Keer R, *et al*. (eds). Shaker Publishing B.V., 1998; 187–194.
13. Yan AM, Nguyen DH. Shakedown of structures by improved Koiter's theorem. *Proceedings of 4th National Congress on Theoretical and Applied Mechanics*, Leuven, Belgium, 22–23 May, 1997; 449–452.
14. Xue DW. Some results on the theory of cylindrical shells. *Proceedings of International Symposium on Shell & Spatial Structures*, 10–14 November, Singapore, 1997; 887–893.
15. Rodabaugh EC, Geoge HH. Effect of internal pressure on flexibility and stress-intensification factors of curved pipe or welding elbows. *Journal of Applied Mechanics*, Transactions ASME 1957; **79**:1165–1174.
16. Calladine CR. Limit analysis of curved tubes. *Journal of Mechanical Engineering Science* 1974; **16**:85–87.
17. Yan AM, Nguyen DH, Gilles Ph. Practical estimation of the plastic collapse limit of curved pipe subjected to complex loading. *Structural Engineering and Mechanics* 1999; **8**(4), in print.

